

Direct Atomic Simulations of Facet Formation and Equilibrium Shapes of SiC Nanoparticles

Henrik Andersen Sveinsson, Anders Hafreager, Rajiv K. Kalia, Aiichiro Nakano, Priya Vashishta, and Anders Malthe-Sørensen*



Cite This: *Cryst. Growth Des.* 2020, 20, 2147–2152



Read Online

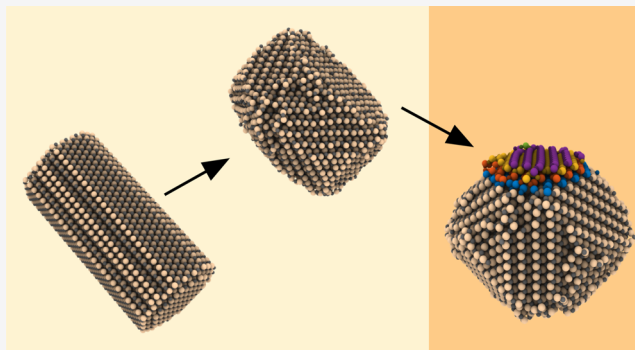
ACCESS |

Metrics & More

Article Recommendations

Supporting Information

ABSTRACT: Understanding the shapes of nanoparticles is an important interdisciplinary problem because particle shapes can affect their properties, functionality, and applications. Advances in nanoscale imaging probes have revealed exquisite details of nanofaceting phenomena. However, quantitative theoretical predictions have not kept up the pace with experimental advances, and the atomic pathways of facet formation are largely unknown due to a lack of direct observations and simulations. Here we examine facet formation in spherical and cubic SiC nanoparticles and in SiC nanowires using molecular dynamics simulations reaching microseconds. We characterize layer-by-layer formation, diffusional motion along edges and corners, and determine energy barriers. We find that the equilibrium shapes are identical regardless of the initial shape of SiC nanoparticles or nanowires. For spherical and cubic nanoparticles, (110) facets form within 10 ns by lateral liquid-like diffusion of atoms. In contrast, faceting in SiC nanowires also involves normal diffusional motion with a higher energy barrier and hence much longer faceting times. These results have important implications for molecular-level understanding of the synthesis and stability of ceramic nanocrystals and nanowires.



INTRODUCTION

Ceramic nanocrystals such as SiC are widely used in electronics,¹ photonics,² biosensors, drug delivery,^{3,4} and structural applications.⁵ Silicon carbide is attractive due to its high mechanical strength. Accordingly, mechanisms and transitions during mechanical loading of silicon carbide have been studied in experiments^{6,7} and molecular simulations.^{8–11} On the nanoscale, the shape of crystals directly affects their properties.^{12–15} Despite advances in nanoscale imaging^{16–20} and modeling, the detailed atomic mechanisms of nanocrystal formation has not been directly observed in experiments or simulation.^{16,21,22} The transformation of a crystalline particle from any initial shape to its equilibrium crystal shape involves a series of complex processes.^{23–26} The final equilibrium shape has facets resulting from the minimization of surface free energy for a given volume.²⁷ The equilibrium shape of a nanocrystal is uniquely determined by the Wulff construction²⁸ according to the surface free energy associated with all crystal directions, resulting in certain planes being preferred. For instance, the expected equilibrium shape for a crystal with (110) planes having the lowest surface energy is a rhombic dodecahedron, possibly truncated by other facets if they have sufficiently low surface energy to intersect at the edges or corners. At finite temperature, a facet can grow in either the lateral or normal direction via the formation of steps and kinks.

The latter results from the diffusion of adatoms from edges and corners.²⁹ The edges and corners between facets can become rounded, but the dominant facets remain intact.³⁰

The formation of a fully grown step or layer may require multiple events to occur, and involve energy barriers that prevent the particle from reaching its equilibrium shape if the surface area of the facet is sufficiently large.^{31,32} In the absence of step-producing defects, Mullins³² has shown that the nucleation energy for growing layers on a facet is prohibitively large and the particle may become kinetically immobilized if the facet is larger than a nanometer. Kinetic Monte Carlo simulations have revealed a similar nucleation barrier.³³ However, the detailed atomic mechanisms of facet formation in nanocrystals have not yet been observed experimentally or computationally with a model where all atomistic mechanisms are available. In this article, we show that facet formation on a ceramic, silicon carbide, can be obtained in direct molecular

Received: May 8, 2019

Revised: January 29, 2020

Published: January 30, 2020

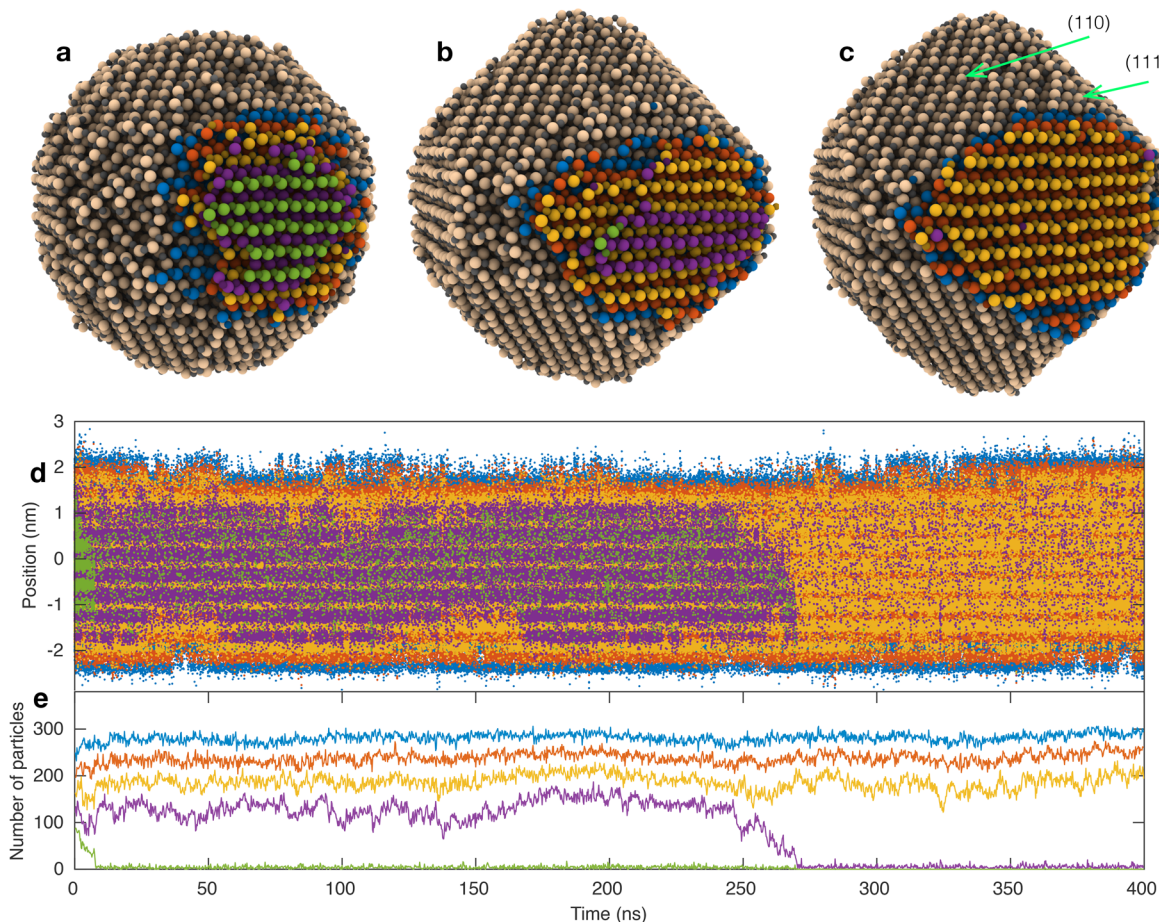


Figure 1. Faceting of silicon carbide nanoparticles. (a–c) Snapshots of silicon carbide nanoparticle (n-SiC) with diameter 8 nm faceting during a molecular dynamics simulation. (a) Initial configuration taken at 0.02 ns, (b) partly faceted particle after 139 ns, and (c) fully faceted particle after 400 ns. In (b) and (c), we see (110) facets, and also island-like (111) facets. In the final configuration, the mean distance from the center of the particle to the (110) planes is 3.73 nm and to the (111) plane 3.90 nm, which by Wulff construction gives the ratio of surface energies $E_{110}/E_{111} = 0.956$, and that the equilibrium shape is a rhombic dodecahedron truncated by a regular octahedron. Colors in (a–c) indicate layer depth on one of the (110) facets, and correspond to the colors in (d,e). (d) scatters the height distribution of particles in the 5 top layers of the crystal through time, and shows that the interplay between rows on the facet is important in the faceting process. (e) shows the numbers of particles in each layer of the colored facet through time, and guides the interpretation of (d). (d,e) only shows the number of atoms in the crystal layers on the facet indicated by colors in (a–c), and thus, even though the number of atoms of the particle as a whole is conserved, the number of atoms in (e) is not conserved.

dynamics simulations, and study the detailed mechanisms involved in the faceting process.

RESULTS AND DISCUSSION

Here we examine how spherical, cubic, and cylindrical silicon carbide nanoparticles in vacuum undergoing volume-preserving shape changes reach the same equilibrium shape by different dynamical mechanisms, crossing significantly different energy barriers over time scales varying by 3 orders of magnitude. Figure 1 shows how a (110) facet forms in an SiC particle that was initially a sphere of diameter 8 nm. Figure 1a shows the onset of facet formation in the spherical SiC nanoparticle at $T = 2200$ K after 0.02 ns. The different colors indicate the layer depth: atoms in the first five layers from the top are colored blue, red, yellow, purple, and green. In the early stages, Si and C atoms diffuse in these layers to expose (110) facets. The diffusion coefficients for Si and C atoms in the early stages of facet formation are close to 7×10^{-6} cm²/s and 1.0×10^{-5} cm²/s, respectively. Figure 1d,e indicates that the participation of the topmost layer (green) in the facet growth ceases after a short duration of less than 10 ns. The snapshot in

Figure 1b shows partial formation of a (110) facet after 139 ns. Atoms in the second layer (purple) participate in the facet growth for another 125 ns and subsequently their participation tails off to zero after 265 ns. These atoms are mostly in the central part of the facet, and they are surrounded by atoms in the third layer. Atoms in the bottom two layers (red and blue) participate in the edges between facets. The snapshot in Figure 1c shows a fully grown (110) facet after 400 ns. Atoms in the bottom two layers (blue and red) continue to diffuse, mostly at the edges and corners of the facet, even after the facet growth stops. The participation of atoms from the bottom three layers remains nearly constant over the entire duration of facet formation; see Figure 1e. After 400 ns, the SiC nanoparticle is transformed from a sphere to faceted nanocrystal with 12 (110) and 8 (111) facets. These are all the (110) and (111) facets that combinatorics on the Miller indices allow for, and it is a different set of facets than those appearing for example in simulations of platinum nanoparticles,³⁴ which has (111) and (100) facets. According to the Wulff construction, this means that these substances have different ratios of surface energies between their (100), (110), and (111) crystal surfaces.

Between the facets on the n-SiC, there are edges and corners along which surface Si and C diffuse with diffusion constants around $3.1(2) \times 10^{-6}$ cm²/s and $4.4(3) \times 10^{-6}$ cm²/s, respectively.

To examine the effect of the initial nanocrystal shape, we also simulated a cubic nanocrystal with length 8 nm and faces in the (001) directions, and a cylindrical nanocrystal of diameter 4 nm and length 8 nm along the [011] crystal direction. These were also performed at $T = 2200$ K. The particle shapes are nearly identical for the sphere and the cube after 1 μ s, but the cylindrical particle differs. Figure 2 shows the

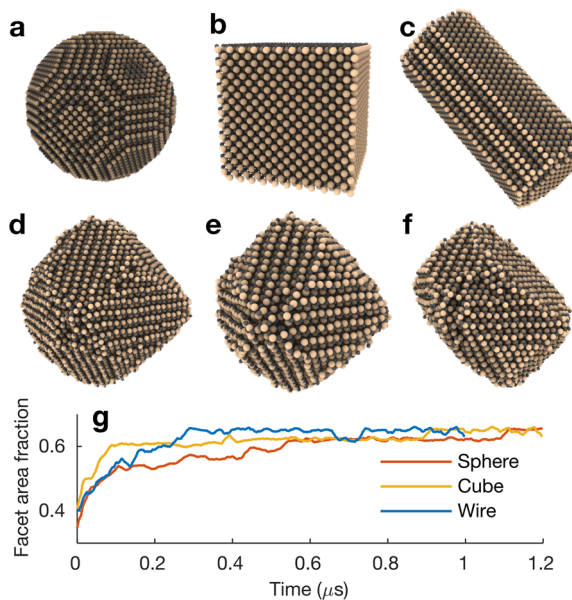


Figure 2. Effects of changing the initial shape of n-SiC. A spherical particle (a) and a cubic particle (b) facets to the same shape (d,e) during simulation at 2200 K. A cylindrical particle (c) does not reach the same shape, and is locked into a metastable shape (f). (g) shows the evolution of the sum of the (110) and (111) facet area through time, and shows that all particles have reached a steady state during the simulation time.

initial shapes (a–c), the final shapes (d–f), and the fraction of the surface area being (110) or (111) facets (g) for the sphere, the cube, and the cylinder. Just like the sphere, the cube transforms into a nanocrystal with 12 (110) and 8 (111) facets. In Figure 2g, we use the facet area fraction as an indication of the facet formation. We observe that this fraction stabilizes in 0.1 μ s for the cube and 0.6 μ s for the sphere. The cylindrical nanoparticle also develops (110) and (111) facets, and its facet area fraction stabilizes after 0.3 μ s, but the shape of this nanoparticle is different from the other ones even after 1 μ s. Note that the faceting times are not directly comparable since the nanoparticles have different volumes.

To investigate the faceting of the cylindrical nanocrystal in more detail, we plot the distance between opposing (110) planes. This, along with snapshots of the particle at various stages of the facet formation, is shown in Figure 3. We again observe the initial faceting phase of 0.3 μ s. During this time, pairs of facets inclined with respect to the major axis move closer to each other, reaching approximately the same value (5.5 nm) after 0.1 μ s. The planes normal to the major axis converge to a higher separation distance (6.3 nm) after 0.3 μ s. However, the distance between the facet pair parallel to the

major axis remains constant through 1 μ s at 2200 K. These are the largest facets. The volume freed by facet pairs only moving toward each other is taken up as lateral growth of facets, ultimately resulting in the formation of corners. Lateral movement and facet area growth result in the formation of two relatively sharp (100) corners, which can be seen in the snapshot after 1 μ s.

The oblate shape of the nanocrystal has to be metastable because it is asymmetric in the (110) planes. Contrary to the sphere and the cube, the cylinder has reached a shape where it cannot get closer to the equilibrium shape by removing atoms from a layer and using them for lateral growth of other facets. It has to grow new layers on top of the largest facets to get closer to equilibrium, and at this point, it seems stuck in a metastable state. In order to kick the system out of its metastable shape, the temperature is raised to 2361 K to see whether it reaches the equilibrium shape. This heating causes a shape change, as can be seen in the shaded part of Figure 3. After 200 ns at 2361 K, all facet pairs converge to same separation distance, and the particles reach the equilibrium shape. The dark blue facet pair takes about 0.2 μ s before it also converges to the same separation distance 5.5 nm. The nanocrystal shape is monitored for 0.6 μ s at 2361 K, and we do not observe any changes in the shape of the nanocrystal. The final shape resembles the final shapes of nanocrystals with spherical and cubic initial configurations.

The oblate shape is metastable due to an energy barrier to the normal motion of sufficiently large facets. To estimate the magnitude of this barrier, we measure the growth rate in 63 simulations at varying temperatures between 2275 and 2385 K. These simulations were run between 200 and 500 ns depending on the time needed to grow new layers. We monitor the time dependence of the number of atoms on top of the largest (110) facet in all of these simulations to determine the nucleation time for new layers on the facet as a function of layer depth and temperature. This number abruptly grows when a new layer is nucleated, so it is sharply defined. Figure 4a,b shows how this number develops for four layers growing in a simulation at 2295 K. Figure 4c shows the waiting times for a single layer height for all simulations. From this Arrhenius plot, we estimate the energy barrier for each layer height; see Figure 4d. This barrier is estimated to 14 eV for the first four layer heights on top of the metastable oblate shape.

CONCLUSIONS

This study demonstrates that processes such as faceting and crystal growth can be within the reach of microsecond molecular dynamics simulations. Here, we have provided insights into the detailed faceting mechanisms of SiC. The results and methods are of general importance in the synthesis of nanocrystals and nanowires. Other materials and processes should be studied using similar approaches to gain insight into what mechanisms are general and what are specific to SiC. Molecular dynamics studies of faceting also open up for more detailed studies of crystal growth procedures and how they are related to the resulting nanocrystal geometry.^{16,21} They may also let us address competing processes between crystal growth and deformation during healing and recrystallization of faceting systems experiencing external mechanical forcing.

METHODS

Si-3C was prepared with a lattice constant of 4.358. To prepare initial nanocrystals, we created a block of bulk SiC-3C in a cubic

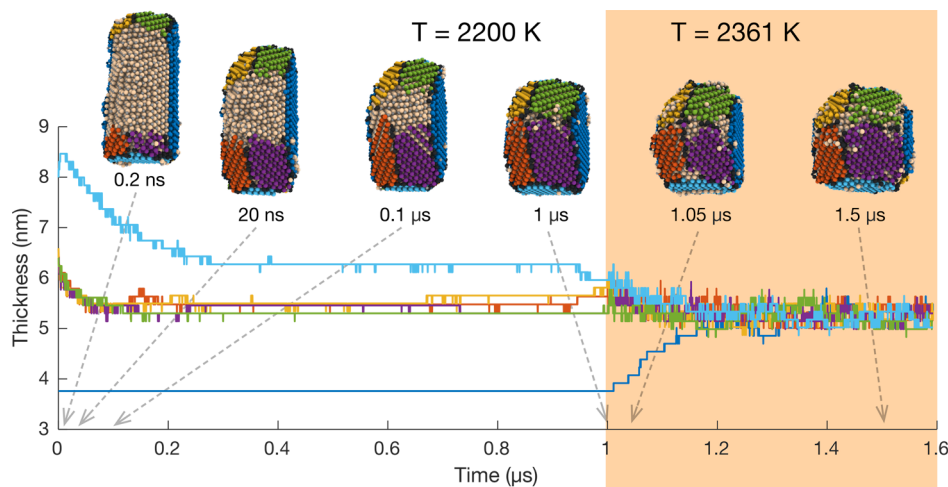


Figure 3. Distance between facet pairs. Snapshots of (110) facets in different directions during a simulation taken at 0.2 ns, 20 ns, 0.1 μ s, 1.05 μ s, and 1.5 μ s. Lines show the distance between opposing facets, and line colors correspond to the colors indicated on the snapshots. The lines are step-like because the removal or addition of a layer results in a discontinuous change in the distance between facets. During the first 1 μ s of the simulation, the distance between most facet pairs decreases, but for the major facet pair (dark blue), we do not observe any layer growth or shrinking, although their areas have increased. Upon heating, new layers grow on the major (110) facet, and the particle reaches its equilibrium shape. The distance between the major planes is constant throughout the first 1 μ s, whereas both the cap plane distance and the minor facet distance are decreasing. In the final state, the distance between all pairs of parallel facets converge to the same value. The yellow, green, red, and purple facets are the inclined, the light blue are the normal, and the dark blue are the parallel facets with respect to the cylinder major axis.

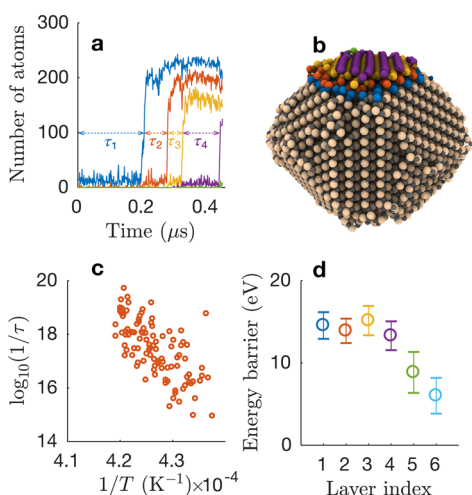


Figure 4. Facet layer growth on the major (110) plane of heated metastable silicon carbide nanoparticles. (a) Layer growth, i.e., the number of atoms, in the first four layers after heating the metastable particle achieved after 1 μ s at $T = 2200\text{ K}$ to $T = 2295\text{ K}$. The waiting times τ_1, \dots, τ_4 for the four layers are indicated in the figure. The colors in (a) correspond to the layers indicated in (b). (c) $\log(1/\tau)$ vs $1/T$ gives the Arrhenius plot for the growth of the second (red) layer. Each marker in (c) corresponds to a full simulation of 200–500 ns. A linear fit to this Arrhenius plot gives the energy barrier for the second layer. Following the same procedure, we obtain the energy barrier for layer formation for the first six layers (d). Error bars in (d) indicate 67% confidence bounds of linear fits to Arrhenius plots.

simulation box of $(40\text{ nm})^3$ (sphere), $(30\text{ nm})^3$ (cube), or $(23.4\text{ nm})^3$ (cylinder), and then deleted atoms that were outside the region defined by the geometrical shape of that initial nanocrystal. This method can lead to nonstoichiometry, which we amended by adding particles to the void to regain stoichiometry. We performed molecular dynamics simulations of the silicon carbide nanocrystal (see, e.g., ref 35 for best practices of MD simulations). We used a force field consisting of two-body and three-body terms.³⁶ All simulations were run with periodic boundary conditions using an NVT Nosé–Hoover

type thermostat³⁷ with a damping time of 1 ps. Equations of motion were integrated with the Velocity Verlet scheme using a time step of 2 fs. The simulation box sizes were such that the nanocrystal did not interact with its periodic image. All simulations were run on NVIDIA P100 computing cards using the GPU package in LAMMPS.³⁸ Diffusion coefficients were calculated using the mean squared displacement of the top three surface layers over 100 ps.

ASSOCIATED CONTENT

Supporting Information

The Supporting Information is available free of charge at <https://pubs.acs.org/doi/10.1021/acs.cgd.9b00612>.

Brief descriptions of how the energy barriers for normal growth on facets were measured, and details of facet evolution on cylindrical n-SiC ([PDF](#))

AUTHOR INFORMATION

Corresponding Author

Anders Malthe-Sørensen — *The Njord Centre, Department of Physics, University of Oslo, NO-0316 Oslo, Norway;*
orcid.org/0000-0001-8138-3995; Email: malthe@fys.uio.no

Authors

Henrik Andersen Sveinsson — *The Njord Centre, Department of Physics, University of Oslo, NO-0316 Oslo, Norway*

Anders Hafreager — *The Njord Centre, Department of Physics, University of Oslo, NO-0316 Oslo, Norway*

Rajiv K. Kalia — *Collaboratory for Advanced Computing and Simulations, University of Southern California, Los Angeles, California 90089-0241, United States*

Aiichiro Nakano — *Collaboratory for Advanced Computing and Simulations, University of Southern California, Los Angeles, California 90089-0241, United States*; *orcid.org/0000-0003-3228-3896*

Priya Vashishta — *Collaboratory for Advanced Computing and Simulations, University of Southern California, Los Angeles,*

California 90089-0241, United States;  orcid.org/0000-0003-4683-429X

Complete contact information is available at:
<https://pubs.acs.org/10.1021/acs.cgd.9b00612>

Notes

The authors declare no competing financial interest.

ACKNOWLEDGMENTS

R.K., A.N., and P.V. were supported by the U.S. Department of Energy, Office of Science, Basic Energy Sciences, Materials Science and Engineering Division, Grant # DE-SC0018195. The simulations were performed at the Argonne Leadership Computing Facility under the DOE INCITE program, at the Center for High Performance Computing of the University of Southern California, at the University of Oslo and using NOTUR grant NN9272K. Researcher exchange was financed by the Norwegian Research Council INTPART grant 250140.

REFERENCES

- (1) Capano, M. A.; Trew, R. J. Silicon Carbide Electronic Materials and Devices. *MRS Bull.* **1997**, *22*, 19–23.
- (2) Song, B.-S.; Yamada, S.; Asano, T.; Noda, S. Demonstration of two-dimensional photonic crystals based on silicon carbide. *Opt. Express* **2011**, *19*, 11084–11089.
- (3) Yakimova, R.; Jr, R. M. P.; Yazdi, G. R.; Vahlberg, C.; Spetz, A. L.; Uvdal, K. Surface functionalization and biomedical applications based on SiC. *J. Phys. D: Appl. Phys.* **2007**, *40*, 6435.
- (4) Saddow, S. E. In *Silicon Carbide Biotechnology*, 2nd ed., Saddow, S. E., Ed.; Elsevier, 2016; pp 1–25.
- (5) Zhao, J.-C.; Westbrook, J. H. Ultrahigh-Temperature Materials for Jet Engines. *MRS Bull.* **2003**, *28*, 622–630.
- (6) Yoshida, M.; Onodera, A.; Ueno, M.; Takemura, K.; Shimomura, O. Pressure-induced phase transition in SiC. *Phys. Rev. B: Condens. Matter Mater. Phys.* **1993**, *48*, 10587–10590.
- (7) Tangpatjaroen, C.; Grierson, D.; Shannon, S.; Jakes, J. E.; Szlufarska, I. Size dependence of nanoscale wear of silicon carbide. *ACS Appl. Mater. Interfaces* **2017**, *9*, 1929–1940.
- (8) Shimojo, F.; Ebbsjö, I.; Kalia, R. K.; Nakano, A.; Rino, J. P.; Vashishta, P. Molecular dynamics simulation of structural transformation in silicon carbide under pressure. *Phys. Rev. Lett.* **2000**, *84*, 3338–3341.
- (9) Szlufarska, I.; Nakano, A.; Vashishta, P. Materials science: A crossover in the mechanical response of nanocrystalline ceramics. *Science* **2005**, *309*, 911–914.
- (10) Chavoshi, S. Z.; Luo, X. Molecular dynamics simulation study of deformation mechanisms in 3C-SiC during nanometric cutting at elevated temperatures. *Mater. Sci. Eng., A* **2016**, *654*, 400–417.
- (11) Sun, S.; Peng, X.; Xiang, H.; Huang, C.; Yang, B.; Gao, F.; Fu, T. Molecular dynamics simulation in single crystal 3C-SiC under nanoindentation: Formation of prismatic loops. *Ceram. Int.* **2017**, *43*, 16313–16318.
- (12) Kinnear, C.; Moore, T. L.; Rodriguez-Lorenzo, L.; Rothen-Rutishauser, B.; Petri-Fink, A. Form Follows Function: Nanoparticle Shape and Its Implications for Nanomedicine. *Chem. Rev.* **2017**, *117*, 11476–11521.
- (13) Murphy, C. J.; Sau, T. K.; Gole, A. M.; Orendorff, C. J.; Gao, J.; Gou, L.; Hunyadi, S. E.; Li, T. Anisotropic Metal Nanoparticles: Synthesis, Assembly, and Optical Applications. *J. Phys. Chem. B* **2005**, *109*, 13857–13870.
- (14) Bruchez, M.; Moronne, M.; Gin, P.; Weiss, S.; Alivisatos, A. P. Semiconductor Nanocrystals as Fluorescent Biological Labels. *Science* **1998**, *281*, 2013–2016.
- (15) Burda, C.; Chen, X.; Narayanan, R.; El-Sayed, M. A. Chemistry and Properties of Nanocrystals of Different Shapes. *Chem. Rev.* **2005**, *105*, 1025–1102.
- (16) Liao, H.-G.; Zhrebetsky, D.; Xin, H.; Czarnik, C.; Ercius, P.; Elmlund, H.; Pan, M.; Wang, L.-W.; Zheng, H. Facet development during platinum nanocube growth. *Science* **2014**, *345*, 916–919.
- (17) Hansen, P. L.; Wagner, J. B.; Helveg, S.; Rostrup-Nielsen, J. R.; Clausen, B. S.; Topsøe, H. Atom-Resolved Imaging of Dynamic Shape Changes in Supported Copper Nanocrystals. *Science* **2002**, *295*, 2053–2055.
- (18) Zheng, H.; Smith, R. K.; Jun, Y.-w.; Kisielowski, C.; Dahmen, U.; Alivisatos, A. P. Observation of Single Colloidal Platinum Nanocrystal Growth Trajectories. *Science* **2009**, *324*, 1309–1312.
- (19) Evans, J. E.; Jungjohann, K. L.; Browning, N. D.; Arslan, I. Controlled Growth of Nanoparticles from Solution with In Situ Liquid Transmission Electron Microscopy. *Nano Lett.* **2011**, *11*, 2809–2813.
- (20) Fei, L.; Ng, S. M.; Lu, W.; Xu, M.; Shu, L.; Zhang, W.-B.; Yong, Z.; Sun, T.; Lam, C. H.; Leung, C. W.; Mak, C. L.; Wang, Y. Atomic-Scale Mechanism on Nucleation and Growth of Mo₂C Nanoparticles Revealed by in Situ Transmission Electron Microscopy. *Nano Lett.* **2016**, *16*, 7875–7881.
- (21) Fichthorn, K. A.; Balankura, T.; Qi, X. Multi-scale theory and simulation of shape-selective nanocrystal growth. *CrystEngComm* **2016**, *18*, 5410–5417.
- (22) Sawada, K.; Iwata, J.-I.; Oshiyama, A. Magic angle and height quantization in nanofacets on SiC(0001) surfaces. *Appl. Phys. Lett.* **2014**, *104*, 051605.
- (23) Herring, C. Some Theorems on the Free Energies of Crystal Surfaces. *Phys. Rev.* **1951**, *82*, 87–93.
- (24) Einstein, T. L. In *Handbook of Crystal Growth*, 2nd ed., Nishinaga, T., Ed.; Elsevier: Boston, 2015; pp 215–264.
- (25) Kitayama, M.; Narushima, T.; Carter, W. C.; Cannon, R. M.; Glaeser, A. M. The Wulff Shape of Alumina: I, Modeling the Kinetics of Morphological Evolution. *J. Am. Ceram. Soc.* **2000**, *83*, 2561–2531.
- (26) Ozdemir, M.; Zangwill, A. Morphological equilibration of a faceted crystal. *Phys. Rev. B: Condens. Matter Mater. Phys.* **1992**, *45*, 3718–3729.
- (27) Gibbs, J. W. *The Collected Works of J. Willard Gibbs*; Yale University Press, 1948; Google-Books-ID: SvQyAQAAIAAJ.
- (28) Wulff, G. Zur Frage der Geschwindigkeit des Wachstums und der Auflösung der Krystallflächen. *Z. Kristallogr. - Cryst. Mater.* **1901**, *34*, 449–530.
- (29) Pimpinelli, A.; Villain, J. *Physics of Crystal Growth* by Alberto Pimpinelli; Cambridge Core - Statistical Physics; Cambridge University Press, 1998.
- (30) Rottman, C.; Wortis, M. Statistical mechanics of equilibrium crystal shapes: Interfacial phase diagrams and phase transitions. *Phys. Rep.* **1984**, *103*, 59–79.
- (31) Mullins, W. W.; Rohrer, G. S. Nucleation Barrier for Volume-Conserving Shape Changes of Faceted Crystals. *J. Am. Ceram. Soc.* **2000**, *83*, 214–16.
- (32) Rohrer, G. S.; Rohrer, C. L.; Mullins, W. W. Nucleation Energy Barriers for Volume-Conserving Shape Changes of Crystals with Nonequilibrium Morphologies. *J. Am. Ceram. Soc.* **2001**, *84*, 2099–2104.
- (33) Combe, N.; Jensen, P.; Pimpinelli, A. Changing shapes in the nanoworld. *Phys. Rev. Lett.* **2000**, *85*, 110–113.
- (34) Wen, Y. H.; Fang, H.; Zhu, Z.; Sun, S. G. Molecular dynamics investigation of shape effects on thermal characteristics of platinum nanoparticles. *Phys. Lett. A* **2009**, *373*, 272–276.
- (35) Braun, E.; Gilmer, J.; Mayes, H. B.; Mobley, D. L.; Monroe, J. I.; Prasad, S.; Zuckerman, D. M. Best Practices for Foundations in Molecular Simulations [Article v1.0]. *Living Journal of Computational Molecular Science* **2019**, *1*, 1–28.
- (36) Vashishta, P.; Kalia, R. K.; Nakano, A.; Rino, J. P. Interaction potential for silicon carbide: A molecular dynamics study of elastic constants and vibrational density of states for crystalline and amorphous silicon carbide. *J. Appl. Phys.* **2007**, *101*, 103515.
- (37) Tuckerman, M. E.; Alejandre, J.; López-Rendón, R.; Jochim, A. L.; Martyna, G. J. A Liouville-operator derived measure-preserving

integrator for molecular dynamics simulations in the isothermal-isobaric ensemble. *J. Phys. A: Math. Gen.* **2006**, *39*, 5629–5651.

(38) Plimpton, S. Fast Parallel Algorithms for Short-Range Molecular Dynamics. *J. Comput. Phys.* **1995**, *117*, 1–19.